A circuit for gradient climbing in *C. elegans* chemotaxis

Johannes Larsch[1,2], **Steven W. Flavell**[1], **Qiang Liu**[1], **Andrew Gordus**[1], **Dirk R. Albrecht**[1,3], and **Cornelia I. Bargmann**[1]

[1]Howard Hughes Medical Institute, Lulu and Anthony Wang Laboratory of Neural Circuits and Behavior, The Rockefeller University, New York, NY 10065, USA

Abstract

Animals have a remarkable ability to track dynamic sensory information. For example, the nematode *Caenorhabditis elegans* can locate a diacetyl odor source across a 100,000-fold concentration range. Here, we relate neuronal properties, circuit implementation, and behavioral strategies underlying this robust navigation. Diacetyl responses in AWA olfactory neurons are concentration- and history-dependent; AWA integrates over time at low odor concentrations, but as concentrations rise it desensitizes rapidly through a process requiring cilia transport. After desensitization, AWA retains sensitivity to small odor increases. The downstream AIA interneuron amplifies weak odor inputs and desensitizes further, resulting in a stereotyped response to odor increases over three orders of magnitude. The AWA-AIA circuit drives asymmetric behavioral responses to odor increases that facilitate gradient climbing. The adaptation-based circuit motif embodied by AWA and AIA shares computational properties with bacterial chemotaxis and the vertebrate retina, each providing a solution for maintaining sensitivity across a dynamic range.

Introduction

Animals use sophisticated sensory systems and behavioral strategies to navigate to favorable conditions in natural environments. The sensorimotor transformations used in animal navigation provide flexible solutions to unpredictable problems, to the extent that design principles derived from animal navigation have inspired biomimetic engineering of autonomous robots that mimic their spatial computations (Benhamou and Bovet, 1989; Franz and Mallot, 2000). Chemosensory cues – odors and tastes – are produced by all living organisms, and provide critical information about nutrients, competitors, mates, and predators. However, they are highly variable in their composition and in their distribution over time and space. Substantial effort has been devoted to understanding the biochemical recognition of odors and tastes by large superfamilies of G protein-coupled receptors (in mammals and nematodes) and ion channels (in insects) (Bargmann, 2006). Complementary

studies have identified higher-order behavioral strategies for tracking odors in gradients (Iino and Yoshida, 2009), in complex plumes (Atema, 1995; Riffell et al., 2008), or across discontinuous boundaries (Vergassola et al., 2007). These two levels of analysis, however, are only incompletely linked to each other by circuits that connect sensory detection with behavioral strategy.

The nematode worm *C. elegans* uses multiple strategies to orient its movement to volatile odors, water-soluble tastes and temperature. One strategy is a biased random walk reminiscent of bacterial chemotaxis (Berg and Brown, 1972). *C. elegans* locomotion alternates between relatively straight forward runs and sporadic "pirouettes" that change the direction of movement (Pierce-Shimomura et al., 1999). Animals in odor gradients prolong runs when moving towards attractants and increase pirouettes when moving away from the attractants by detecting changes in concentration over time (dC/dt) (Pierce-Shimomura et al., 1999). These behaviors can be recapitulated in response to purely temporal odor pulses in microfluidic environments (Albrecht and Bargmann, 2011). In a second strategy, animals can orient their steering during forward movement to move directly toward an odor source, the "weathervane" behavior (Iino and Yoshida, 2009). Oriented steering appears to result from active sensing in which olfactory signals are temporally coupled with head sweeps during ongoing sinusoidal movement (Izquierdo and Lockery, 2010; Kato et al., 2014).

A challenge for chemotaxis using either strategy is the variation in environmental odor levels experienced as an animal tracks an odor. For example, a point source of the odor diacetyl attracts *C. elegans* over a 100,000 fold concentration range (Bargmann et al., 1993), implying that the underlying sensory systems can maintain sensitivity to odor fluctuations across this range. One mechanism that can prevent saturation at high odor levels is adaptation, a resetting of responsiveness based on sensory history that has been observed in essentially all sensory systems, including bacterial chemosensation (Berg and Brown, 1972), invertebrate and vertebrate olfaction (Reisert and Zhao, 2011; Wilson, 2013), and vision (Montell, 2012; Rieke and Rudd, 2009). In addition to extending the dynamic range of the system, adaptation tunes it to changes in stimulus intensity in preference to absolute stimulus levels, a feature that would promote both biased random walk and steering behavior.

In *C. elegans*, two pairs of ciliated chemosensory neurons called AWA and AWC mediate attraction to volatile odors. Chemotaxis to low concentrations of diacetyl requires the AWA sensory neurons and ODR-10, a G protein-coupled olfactory receptor (Bargmann et al., 1993; Sengupta et al., 1996). Other GPCRs in AWA and AWC are thought to detect other odors. AWA calcium levels increase upon odor addition, suggesting depolarization (Larsch et al., 2013; Shinkai et al., 2011), whereas AWC calcium levels decrease in odor, suggesting hyperpolarization (Chalasani et al., 2007). AWA and AWC have distinct but overlapping synaptic partners: for example AWA forms gap junctions onto AIA interneurons, whereas AWC forms chemical synapses onto AIA (Fig. 1a). These observations suggest that AWA and AWC perform functionally distinct computations even though they both give rise to odor chemotaxis behavior.

Multiple interneurons, including AIA, AIB, and AIY, are regulated by the odors sensed by AWA and AWC and may therefore provide the neuronal substrates that link sensory detection to a behavioral response. The integrating interneurons downstream of AWA and AWC are functionally redundant for chemotaxis in a general sense, but quantitative assays indicate that they have distinguishable functions. For example, AIB interneurons set reversal rates in the biased random walk strategy (Iino and Yoshida, 2009; Luo et al., 2014), and AIY interneurons are required for steering (Satoh et al., 2014), but neither AIB nor AIY is essential for chemotaxis in odor gradients. In this work, we implicate another interneuron, AIA, in the dynamic detection of odor increases, and define the algorithm by which it contributes to chemotaxis behavior.

Establishing the precise relationships between odor distribution, neuronal recruitment and dynamics, and resulting chemotaxis behaviors is challenging. The development of high-throughput, quantitative methods for monitoring neuronal calcium signaling and behavior in *C. elegans* in well-controlled environments provides the opportunity to analyze these features of chemosensory circuits (Albrecht and Bargmann, 2011; Larsch et al., 2013). Here we define properties of AWA sensory neurons and AIA integrating interneurons that allow them to represent a wide range of odor concentrations and concentration changes. We show that these neurons are dynamically tuned to detect odor increases, enabling them to drive a specialized, asymmetric strategy for gradient climbing in chemotaxis.

Results

AWA calcium dynamics are shaped by odor history on multiple time scales

The AWA sensory neuron is essential for chemotaxis to diluted diacetyl on agar plates, but the odor concentrations that the animal experiences in these assays are unknown. To define the relationship between chemotaxis and concentration, we monitored the behavior of *C. elegans* in microfluidic arenas while delivering precise spatial and temporal patterns of diacetyl odor in an all-liquid environment (Albrecht and Bargmann, 2011) (Figure 1b, Movie S1). Chemotaxis to diacetyl was assayed in sigmoidal odor gradients in which animals controlled their own sensory experience by moving in the gradient, as they do during chemotaxis on agar plates. Wild-type animals preferentially migrated towards peak diacetyl concentrations from 11 nM to 115 μM, showing peak accumulation within five minutes and then dispersing slightly over the following ten minutes (Figure 1c; for simplicity, approximate odor concentrations will be used in the text). Mutant animals lacking the AWA diacetyl receptor ODR-10 did not chemotax when the peak diacetyl concentration was below 10 μM, indicating that ODR-10 and by implication AWA are required for chemotaxis in the nanomolar to low micromolar range (Figure 1c). AWA forms synapses with multiple sensory neurons and interneurons, including AIA (Figure 1a). When AIA interneurons were silenced by expression of the leaky potassium channel *unc-103(gf)* (Peterson et al., 2004), chemotaxis to diacetyl was less precise (Figure 1c). The contribution of AIA to AWA-dependent behavior is considered further below.

To relate neuronal responses to behavior, a similar microfluidic device was used to monitor odor-evoked neuronal activity in animals expressing genetically-encoded calcium indicators in the GCaMP series (Akerboom et al., 2012; Larsch et al., 2013; Tian et al., 2009)(Figure

2a). Diacetyl pulses from 1 nM – 100 μM elicited transient, dose-dependent calcium increases in AWA sensory neurons that were strongly dependent on odor concentration and stimulus duration (Figure 2b). Reponses to a 30 s pulse of 1–10 nM diacetyl were weak, but persisted through the stimulus; responses to 100 nM–10 μM diacetyl peaked within ten seconds and then decreased during stimulation; responses to 100 μM diacetyl did not decrease. These concentration- and history-dependent AWA decreases are defined as desensitization. Desensitization had characteristic rates at each concentration (Figure 2c), and was incomplete. For example, at 1 μM diacetyl, AWA calcium fell in one minute to a low steady-state level that was maintained for at least five minutes (Figure 2d). Thus the AWA response to behaviorally relevant diacetyl concentrations includes a strongly desensitizing range.

When 30 s pulses were delivered once per minute, AWA responses fell in each successive trial, an effect that was strongest at 100 nM (Figure 2e,f). This decrease between trials, defined as habituation, was observed even for low diacetyl concentrations that did not desensitize within a trial. Habituation rescaled response magnitude but largely preserved the desensitization characteristics of each odor concentration (Figure 2e,f). Habituation was strong across the first few trials, but diminished thereafter. For example, in a five hour experiment in which animals were pulsed once per minute with 1 μM diacetyl for 5 s, the magnitude of AWA calcium responses fell rapidly during the first seven odor pulses, then slowly over the next ~300 pulses (Figure 2g). Other odor stimuli and patterns showed the same two phases of AWA habituation (data not shown).

In combination, these experiments demonstrate effects of odor history on AWA calcium responses at multiple timescales: rapid concentration-dependent desensitization that begins within a few seconds of odor onset, and at least two forms of habituation with different kinetics.

The relationship between voltage, calcium and GCaMP responses in AWA neurons

A variety of biochemical processes fall between diacetyl detection and GCaMP signals in AWA neurons: the activation of the ODR-10 receptor and subsequent G protein pathways, depolarization and calcium entry through the TRPV sensory transduction channel, signal amplification through voltage-gated calcium channels in the cell body, calcium extrusion, and calcium-to-fluorescence conversion by GCaMP. In principle, any of these processes could change during AWA desensitization.

To distinguish whether desensitization occurs upstream and downstream of voltage changes, we used the red-shifted Chrimson variant of Channelrhodopsin (Klapoetke et al., 2014) to directly depolarize AWA while recording calcium signals with GCaMP2.2b (Figure 3a). Electrophysiological recordings of Chrimson-expressing AWA neurons under current clamp demonstrated that red light induced rapid depolarization that was stable during a 10- or 30-second stimulation and quickly returned to the resting membrane potential after light shutoff (Figure 3b). Chrimson activation with red light also induced saturable GCaMP calcium increases in AWA, with a similar peak magnitude as those induced by odor (Figure 3c). This depolarization-induced fluorescence rose with a t½ of 1 s, desensitized during sustained

illumination with a t½ of 25 s, and decayed after the end of the stimulus with a t½ of 5 s (Figure 3c–e, S3).

Odor concentrations above 100 nM resulted in AWA calcium increases with a rapid rise time consistent with depolarization (Figure 3c, S3). Odor removal led to a decay in calcium signals with a t½ of 5s, the same as observed at the end of Chrimson illumination (Figure 3d,e). Identical rates of post-odor fluorescence decay were observed across different odor concentrations, durations of odor exposure, and calcium levels (Figure 3d, S3). These results indicate that odor removal and Chrimson shutoff are equivalent with respect to this sensor, and suggest that odor removal triggers a voltage decrease in AWA followed by a fixed rate of calcium efflux.

In the presence of sustained odor, however, AWA responded differently than under sustained Chrimson illumination. Near 1 μM diacetyl, calcium fell with a t½ of 7.5 seconds, almost as quickly as when odor was removed. A similar rapid calcium decay was observed with 100 nM odor but not at higher or lower concentrations, even when peak signals were the same (eg 1 and 10 μM odor)(Figures 2,3). The distinct decay patterns with Chrimson and different odor concentrations suggest that desensitization cannot be explained purely by uncoupling calcium from voltage, or by increased calcium efflux. A consistent single explanation for these results is that AWA desensitizes to intermediate odor concentrations at a step in olfactory transduction before cell body depolarization. The AWA responses to odor and Chrimson began to diverge within the first second of the calcium trace, suggesting that desensitization is initiated within this time.

By testing different calcium sensors and conditions we considered how technical properties of GCaMPs and reporter strains limit the sensitivity and time resolution of these experiments (Figure S1). Desensitization to intermediate odor concentrations was robust, and observed with all sensors.

Intraflagellar transport proteins (IFT) and inositol phospholipids regulate AWA desensitization and habituation

To define the molecular requirements for AWA odor detection and desensitization, mutant strains were examined, beginning with genes that affect sensory transduction (Figure 4a, S2). AWA calcium transients in *odr-10* mutants were reduced >1000-fold in sensitivity, confirming ODR-10 as the primary AWA diacetyl receptor (Figure 4a, S2). Calcium responses were absent in *osm-9* and *ocr-1 ocr-2* mutant animals, which disrupt the TRPV transduction channels, and reduced 1000-fold in sensitivity in *ocr-2* single mutants (Figure 4a). AWA calcium responses were strongly reduced in the L-type voltage gated calcium channel mutant *egl-19(n582)*, suggesting that a voltage-to-calcium transformation is essential to the AWA calcium signal.

AWA odor responses, desensitization, and habituation were all normal in mutants for the arrestin homolog *arr-1*, suggesting that arrestin modulation of GPCR signaling is not central to response regulation (Figure S2). Similarly, AWA odor responses were unchanged in the synaptic transmission-defective mutants *unc-18(e234), unc-13(e51)* and *unc-13(s69)* (Richmond et al., 1999; Weimer et al., 2003), suggesting that diacetyl detection,

desensitization and habituation are largely independent of fast synaptic input (Figure S2). A small enhancement of habituation and desensitization was observed in the neuropeptide release-defective mutant *unc-31* and the neuropeptide processing mutant *egl-3*, suggesting a minor role of neuropeptide signaling in response regulation (Figure S2).

We fortuitously discovered a role for intraflagellar transport (IFT) proteins in sensory regulation through studies of the strain CB450, which bears an *unc-13(e450)* mutation and did not show fast desensitization at any odor concentration (Figure 4a, S2). High throughput imaging, linkage analysis, and whole genome sequencing demonstrated that the defect was not caused by the *unc-13* mutation but rather by a linked mutation in *che-3*, which encodes a ciliary dynein heavy chain motor protein that regulates cilium structure (Wicks et al., 2000). Three other IFT mutants, *che-3(e1124), osm-6(p811)*, and *che-2(e1033)*, also failed to desensitize or habituate to diacetyl (Figure 4a,b, S2, S3).

IFT mutations decrease sensory responses in most ciliated sensory neurons (Inglis et al., 2007), but AWA had robust calcium responses across a range of odor concentrations in *che-2, che-3* and *osm-6* mutants (Figure 4a,b), and only mild defects in diacetyl chemotaxis at the concentrations at which AWA is required (Bargmann et al., 1993; Matsuura et al., 2013; Figure S3). All of the IFT mutants had abnormal AWA cilia, in agreement with previous studies (Figure 4c, S3 and data not shown). The defect in *osm-6(p811)* was rescued by AWA-restricted expression of an *osm-6* cDNA (Figure 4a). These results indicate that IFT plays a direct or indirect role in AWA desensitization and habituation.

A defect in AWA dynamics reciprocal to that of the IFT mutants was present in a previously uncharacterized chemotaxis-defective mutant, *ky121* (Roayaie, 1996). *ky121* mutants had diminished responses to diacetyl at low concentrations, and habituated more quickly upon repeated stimulation than wild type (Figure 4a,d); they were also defective in sensory responses mediated by a second neuron, ASH (Figure S4). Linkage analysis and whole-genome sequencing mapped this defect to a missense mutation in the predicted phosphoinositol-5-phosphatase (INPP5) encoded by T25B9.10, *inpp-1*. Two additional *inpp-1* loss-of-function mutants had similar AWA calcium defects (Figure S3). The sensory defect in AWA was rescued either by a genomic fosmid clone covering *inpp-1*, or by AWA-specific expression of cDNAs encoding either of two tested protein isoforms of T25B9.10 (Figure 4a, S3). Thus *inpp-1* acts within AWA to regulate odor responses.

A GFP-tagged INPP-1 protein was widely expressed in neurons, and distributed through the cytoplasm (Figure S4). AWA neurons in *inpp-1(ky121)* mutants appeared normal, with characteristic branched cilia. However, the expression of ODR-10 diacetyl receptors in AWA cilia was subtly altered in *inpp-1* mutant animals, suggesting a possible alteration in receptor localization or cilia structure (Figure S4).

The AIA interneurons respond to diacetyl downstream of AWA and other sensory neurons

To determine how AWA activation is relayed to its synaptic targets, we began with the AIA interneurons that affected diacetyl chemotaxis in microfluidic gradients. AIA calcium responses are largely restricted to the neurites (Chalasani et al., 2010), which responded to diacetyl pulses from 1 nM to 100 μM with transient calcium increases (Figure 5a). AIA

responses to 1–10 nM diacetyl were graded and sustained across a 10 s odor pulse, whereas responses at higher concentrations peaked within 1–3 s of odor onset and then desensitized (Figure 5a). The AIA response in this range was stereotyped in its magnitude and dynamics, varying little between concentrations or across trials (Figure 5a, S5). These results suggest that diacetyl responses in AIA are highly sensitive, saturating, and relatively uniform with respect to odor concentration over a 100-fold range.

A panel of mutants was used to identify the sensory origin of AIA diacetyl responses. In *odr-10(ky32)* AWA diacetyl receptor mutants and in *odr-7(ky4)* mutants defective in AWA development, AIA responses to diacetyl were reduced in magnitude and delayed in onset compared to wild type animals (Figure 5a–c). Thus AWA is responsible for the fast response in AIA, but other sensory neurons also play a role. A possible source of the residual response is the AWC neurons, which support diacetyl chemotaxis at high concentrations (Chou et al., 2001). A *ceh-36(ky646)* mutation that affects the development of AWC and ASEL sensory neurons (Lanjuin et al., 2003) had near-normal AIA calcium responses to diacetyl, but *ceh-36(ky646) odr-7(ky4)* double mutant animals lacked almost all responses, suggesting that the second sensory neuron that senses diacetyl could be AWC or ASEL (Figure 5a–c).

The synaptic connection between AWA and AIA was probed directly by expressing the red-shifted Channelrhodopsin derivative Chrimson in AWA neurons and expressing GCaMP in AIA to record calcium signals. This experiment should minimize contributions of AWC, ASEL, and other unknown sensory neurons to AIA activation (Figure 5d). Chrimson excitation of AWA induced rapid, desensitizing AIA calcium transients that closely resembled those induced by high odor concentrations, indicating that AWA depolarization is sufficient to drive the characteristic short-lived AIA calcium response (Figure 5d).

AWA and AIA respond to fold-change increases in odor concentration

In natural environments, diffusion and convection can generate many odor patterns, but most experimental studies of olfaction use only sharp odor steps. To model graded odor stimuli, we examined AWA and AIA responses to smaller changes resembling those that animals experience in the sigmoidal odor gradient. A sustained 11.5 nM or 115 nM diacetyl stimulus was delivered for ten minutes to define a baseline. Without removing the odor, increasing amounts of diacetyl at a fixed ratio were delivered at one step each minute, with each step representing a 14%, 58%, or 115% increase over the preceding step (a fold-change step, Shoval et al., 2010) (Figure 6a,b). The protocol spanned a range of diacetyl concentrations and concentration changes at which AWA drives chemotaxis behavior (Figure 1b; see Extended Experimental Procedures for detailed comparisons of odor concentrations in behavioral and imaging assays).

When presented with a 14% increase in diacetyl concentration, AWA responded weakly (Figure 6a), but when presented with a 58% or 115% step, AWA responded to each diacetyl increase with a calcium increase (Figure 6a). AWA responses desensitized fully within the 60 s pulse at low concentrations, but did not desensitize fully at concentrations above 500 nM. Even though the AWA response peaked by ~3 μM, desensitization allowed continued detection of increases above this level. This response provides a potential explanation for the

strong desensitization of AWA calcium responses near 1 μM: desensitization allows AWA to respond to diacetyl increases instead of saturating.

AIA interneurons responded to fold-change odor increases with calcium transients that desensitized fully within each pulse (Figure 6b). The fraction of responding AIA neurons changed with the size of the concentration change, such that each animal responded to less than half of the 14% odor steps, but to most 58% steps and 115% steps (Figure 6c). In contrast with AWA, AIA responses to fold-change increases were stereotyped in magnitude and dynamics, regardless of the absolute diacetyl concentration (Figure 6d). Accordingly, AIA had a two-fold lower coefficient of variation than AWA for peak response magnitudes across the tested odor concentrations (Figure 6e). The normalized responses in AIA appeared to report odor increases more accurately than odor concentrations.

AIA responses to diacetyl fold-change increases required the AWA diacetyl receptor ODR-10 (Figure 6b,f), even at concentrations at which AIA could have responded to larger diacetyl steps without AWA or ODR-10 input (Figure 5). Thus AWA is essential for the transmission of fold-change increases to AIA.

AWA and AIA had asymmetric calcium responses to odor increases and decreases. Neither AWA nor AIA responded significantly to small decreases; large decreases (53 μM to 10 nM diacetyl) resulted in a large fall in AWA calcium, with no detectable change in AIA (Figure 6a,b). Thus AWA and AIA are elements of a circuit module that preferentially detects small increases over decreases in odor concentrations.

AWA and AIA suppress turning upon small increases in odor concentrations

In the biased random walk mechanism of chemotaxis, turning rates are suppressed when attractive odors increase and enhanced when they decrease. In agreement with this model, direct depolarization of AWA with Chrimson suppressed spontaneous turning within 5 seconds, and turning off the light after 20 seconds elicited ~10 s of rebound turning (Figure 7a). To ask how fold-change detection by AWA and AIA relates to behavioral functions, we challenged freely-moving animals with fold-change odor upsteps and downsteps in a microfluidic pulse device (Albrecht and Bargmann, 2011)(Figure 7b). Animals were first pre-adapted to 115 nM diacetyl, then exposed to 58% upsteps at 2 minute intervals to a final concentration of 1–2 μM. In wild-type animals each odor fold-change upstep caused a transient suppression of turning, with a minimum at 22 ± 5.5 seconds and a return to baseline over the next 40 s (Figure 7b,c). The magnitude and dynamics of suppression were similar for each step. Fold-change increases were poorly detected by animals mutant for the AWA diacetyl receptor ODR-10 (Figure 7b–d), or by animals with silenced *AIA::unc-103(gf)* interneurons (Figure 7c,d), indicating that AWA and AIA mediate the behavioral response.

In contrast with increases, small decreases in diacetyl concentration across the same concentration range had only a small effect on turning rates (Figure 7b,d). A large odor downstep from 1.82 μM to 115 nM diacetyl increased turning in wild type, but also in *odr-10* and *AIA:unc-103(gf)* animals (Figure 7c,d). The response to a large downstep thus involves a separate circuit. It may be initiated by AWC neurons, which detect both odor

increases and odor decreases, regulate turning bidirectionally, and contribute to diacetyl chemotaxis (Chalasani et al., 2007, Albrecht and Bargmann, 2011, Chou et al., 2001). In summary, the AWA-AIA circuit drives behavioral responses to small fold-change steps whose odor sensitivity, asymmetric preference for increases, and magnitude scaling resemble AIA calcium responses.

Discussion

Sensory circuits across species and modalities have common features that suggest the existence of core circuit motifs and computations. Certain inputs are segregated by polarity: in the retinas of vertebrates and flies, parallel circuits process light onset and light offset (Joesch et al., 2010; Wässle, 2004), and in the olfactory system of *C. elegans*, parallel circuits detect odor addition and removal (Chalasani et al., 2007). Certain inputs are normalized to maintain specificity: at the first olfactory relay of flies and zebrafish, the response to odor quality is maintained across concentrations by inhibitory neurons that normalize activity to total stimulus level (Carandini and Heeger, 2011; Olsen et al., 2010; Zhu et al., 2013). The circuit including the AWA sensory neurons and AIA interneurons represents a dynamic motif that extracts a particular feature of the stimulus, an increase in concentration over time. The circuit's stereotyped, asymmetric response to fold-change odor increases is distinct from the detection of discrete odor pulses, another dynamic computation in olfaction (Fujiwara et al., 2014; Geffen et al., 2009). Above its apparent threshold, the AIA response is only slightly influenced by the magnitude of change or the ambient odor level. At a behavioral level, AIA is required for an asymmetrical turning motif in which small increases in odor concentration transiently suppress turning. The match between AIA calcium responses, AIA-dependent behaviors, and chemotaxis models provides an algorithm for climbing odor gradients, which could be sought in other olfactory systems as well.

Desensitization in AWA requires ciliary transport

AWA calcium responses desensitize and habituate at the odor concentrations at which AWA is required for chemotaxis. Rapid desensitization endows AWA with the ability to respond repeatedly to successive small increases in odor concentration, and to detect changes over a wide range of stimulus intensities without saturation. Desensitization is reduced at very high diacetyl concentrations, which may explain previous observations that AWA is less effective at guiding chemotaxis to high diacetyl than AWC, a less sensitive neuron (Chou et al., 2001). Desensitization may also enable processes such as novelty detection, acute protection from overstimulation, or sharpening of response dynamics for efficient downstream processing (Wark et al., 2007). Interestingly, desensitization is observed in other *C. elegans* sensory neurons whose calcium levels increase with stimulation, like AWA, but is less prominent in sensory neurons whose calcium levels decrease with stimulation, like AWC (Chalasani et al., 2007; Hilliard et al., 2004; Suzuki et al., 2008; Wakabayashi et al., 2009). The depolarizing regime of sensory processing may preferentially encode stimulus change over stimulus level, and may help explain why AWA and AWC, which detect similar and even overlapping attractive odors, have distinct sensory transduction properties.

Calcium is only one facet of a neuron's activity, and therefore this view of desensitization is necessarily incomplete. Neuronal calcium is more closely related to the neuronal output than input, and its dynamics are slow; the time resolution of the signal measured here is limited to about 1–2 s, and likely underestimates the real speed and complexity of AWA signaling (Neher, 1995; Hires et al., 2008; Figure S1). More precise temporal information awaits electrophysiological studies of AWA odor responses. Nonetheless, AWA desensitization to odor is observed using different sensors and conditions, is always strongest at intermediate odor concentrations around 1 μM, and closely resembles the response to a voltage decrease, suggesting that it is a robust phenomenon reflecting intrinsic AWA activity. Perhaps most importantly, calcium desensitization made the unexpected prediction that AWA would preferentially report odor increases over decreases, a prediction borne out in behavioral experiments.

Desensitization and rapid habituation in the AWA neurons require ciliary genes for intraflagellar transport (IFT). Primary odor responses in AWA did not require IFT proteins, a notable result because most sensory neurons are much less sensitive in IFT mutants, in keeping with their structurally abnormal cilia (Inglis et al., 2007). Although the relatively insensitive GCaMP2.2b indicators would not detect all responses, it is nonetheless evident that IFT mutations affect desensitization mechanisms in AWA more strongly than they affect odor detection. Desensitization may require specific proteins that are normally transported to AWA cilia by IFT, or it may depend more generally upon normal cilia morphology. More speculatively, desensitization could result from acute IFT-dependent translocation of signaling molecules in AWA cilia. The IFT speed of ~0.4 um/sec would easily support movement of molecules through the ~5 uM-long AWA cilia branches, and acute translocation has precedent in *Drosophila* photoreceptors, where several molecules including the TRPL channel are translocated through sensory microvilli during light adaptation (Bähner et al., 2002). The AWA TRPV channel encoded by *osm-9* and *ocr-2* undergoes IFT-dependent transport in other ciliated neurons (Qin et al., 2005), so these channels are candidates for active regulation by IFT.

Regardless of the exact mechanism, the requirement for IFT suggests that AWA desensitization involves the cilia, the site of GPCR signaling. Candidates for regulation include the ODR-10 receptor itself or G protein regulators such as RGS proteins (Krzyzanowski et al., 2013), in addition to TRPV channels. An early site of desensitization, upstream of the essential voltage-activated calcium channel *egl-19*, is also consistent with the weak desensitization when AWA is directly depolarized with Chrimson.

inpp-1 mutants had accelerated habituation to diacetyl, suggesting that inositol phospholipids regulate AWA dynamics. Inositol phospholipids regulate the TRPV channel family (Lukacs et al., 2007), as well as membrane traffic and particularly endocytosis (Di Paolo and De Camilli, 2006), which might relate to the subtle changes in ODR-10 localization observed in mutants. The closest human homolog of *inpp-1* affects the stability of primary cilia, and mutations in this gene can cause Joubert syndrome, a ciliopathy affecting midbrain development (Bielas et al., 2009; Jacoby et al., 2009).

AIA interneurons are specialized to detect small odor increases

The AIA interneurons compressed the richness of AWA dynamics across diacetyl concentration and history into calcium signals with stereotyped magnitudes and dynamics. Although the normalized AIA response appears to discard information about absolute odor levels that are represented in AWA, additional information can be transmitted to other AWA synaptic partners (Figure 1) to allow multiple computations.

AWA and AIA neurons are connected only by gap junctions in the *C. elegans* wiring diagram, suggesting that they communicate via electrical synapses. The calcium response in AIA is an indirect and delayed representation of activity, but can nonetheless provide some information about the relationship between these neurons. For example, the rapid desensitization of AIA calcium compared to AWA is consistent with three possibilities: shunting of AWA voltage upstream of the gap junction, which seems unlikely as *C. elegans* neurons are believed to be isopotential (Goodman et al., 1998), filtering of AWA signals or active regulation by the gap junctions (Bloomfield and Völgyi, 2009), or intrinsically desensitizing dynamics in AIA.

The AIA response can be understood in the context of the biased random walk model for *C. elegans* chemotaxis: the model's dependence on dC/dt, rather than absolute odor concentration, is most effectively implemented by concentration-dependent adaptation in the chemotaxis circuit. Adaptation serves as an effective solution for maintaining response sensitivity over a wide input range, a dilemma sometimes called the 'sensitivity paradox' in *E. coli* chemotaxis (Sourjik, 2004). The asymmetry, amplification, and stereotypy of the AWA-AIA connection create a possible solution for the sensitivity paradox. Through these processes, small changes in diacetyl concentrations are preferentially sensed and acted upon when diacetyl concentrations rise, a result reminiscent of the bacterial chemotaxis strategy, where turning is suppressed by small increases in attractant concentration but unchanged by small decreases (Berg and Brown, 1972). In both *E. coli* chemotaxis and *C. elegans* diacetyl chemotaxis, sufficiently large decreases in attractants stimulate turning, so the asymmetry is not absolute. It is instructive to compare these results to *C. elegans* salt chemotaxis behavior, where turning rates are symmetrically regulated by concentration increases and decreases (Kunitomo et al., 2013; Luo et al., 2014). The problem solved during salt chemotaxis does not invoke the sensitivity paradox, as the 4-fold (25–100 mM) salt concentration range of this behavior does not require the extreme adaptation required over a 10^5-fold range of diacetyl concentrations.

The sensitivity paradox also applies to the vertebrate visual system, where rod or cone photoreceptor pathways can each maintain sensitivity over 10^6-fold variations in luminance. Like adaptation to diacetyl, adaptation to ambient luminance involves both desensitization within receptor cells and adaptation in downstream bipolar-amacrine cell circuits (Dunn et al., 2007; Ke et al., 2014). However, the logic and details of the systems differ. The most sensitive adaptation in the retina is in downstream circuits (Dunn et al., 2007), whereas the most sensitive adaptation to diacetyl occurs in the AWA sensory neurons. Therefore, while luminance adaptation in the retina, diacetyl adaptation in AWA and AIA, and intracellular adaptation in bacterial chemotaxis perform functionally related computations, they are executed by different mechanisms.

AIA neurons suppress turning when AWA detects diacetyl increases, and also suppress spontaneous turning induced by AWC olfactory neurons and ASK gustatory neurons (Chalasani et al., 2007). More complex roles for AIA include integrating positive and negative chemical cues in ambiguous environments, and providing neuropeptide feedback to AWC for odor adaptation (Chalasani et al., 2010; Shinkai et al., 2011). These individual examples share some features; for example, the net effect of AIA activity in each case decreases turning. However, the overall effect of the AIA interneuron is determined by the circuit context in which it appears, and as a result AIA can even seem to have opposite valences – AIA enhances chemotaxis initiated by AWA by suppressing turning, but inhibits chemotaxis initiated by AWC by a negative feedback loop. These results highlight the importance of understanding neural circuits in the context of the computations they perform, considering their relationship to sensory inputs, distinct motor outputs, and the way that behaviors play out over time.

Experimental Procedures

Standard genetic and molecular biology techniques were used. A complete strain list appears in Supplemental Information.

Stimulus preparation and delivery

Odor dilutions were prepared fresh on the day of the experiment from pure stock solutions (2,3-butanedione (diacetyl), Sigma-Aldrich, Product 11038). Dilutions for calcium imaging were made in S-basal buffer containing 1 mM acetylcholine agonist (–)-tetramisole hydrochloride (Sigma-Aldrich, Product L9756) to paralyze body wall muscles and keep animals stationary. Dilutions for behavioral analysis were made in S-basal buffer.

During dose response experiments, 10 s or 30 s odor pulses were delivered every 60 s at a given concentration, with an additional delay of 60 s between different odor concentrations in ascending order, unless otherwise noted.

Calcium imaging and data analysis

Methods followed those described previously (Larsch et al., 2013). Briefly, GCaMP fluorescence was recorded in custom made microfluidic polydimethylsiloxane (PDMS) chambers allowing parallel observation of approximately 20 animals during odor stimulation. Continuous liquid flow through the device and over the animals allowed for rapid exchange of chemical stimuli in less than 1 s. In experiments in which Chrimson was activated during calcium imaging, we mounted an external red LED above the imaging chamber and used an excitation filter to narrow illumination to a 605 ± 25 nM band. Tiff stack movies were acquired on an Andor iXon3 DU-897 EM-CCD or a Hammamatsu Orca Flash 4 sCMOS camera at 10 fps. Neuron fluorescence was analyzed using custom scripts written for ImageJ (Neurotracker), and MATLAB was used for subsequent data analysis and display. Most statistical comparisons were made by ANOVA using the Bonferroni correction for multiple comparisons. Further details are provided in Supplemental Experimental Procedures.

Electrophysiology

AWA neurons were recorded using single-electrode whole-cell current clamp largely as described (Goodman et al., 1998; Liu et al., 2009). An animal was glued to a glass coverslip and a small incision was used to expose the AWA neuron, which was identified by expression of an mCherry reporter.

Supplemental Experimental Procedures (Supplemental Material) include the identification of *che-3(ky1018)* and *inpp-1(ky121)*, scoring of cilia in *inpp-1(ky121)*, and detailed descriptions of microfluidic behavioral assays (odor gradients, odor pulses), comparisons between different microfluidic assays, calcium imaging and analysis, electrophysiology recording conditions, and molecular biology.

Supplementary Material

Refer to Web version on PubMed Central for supplementary material.

Acknowledgments

References

Akerboom J, Chen T-W, Wardill TJ, Tian L, Marvin JS, Mutlu S, Calderón NC, Esposti F, Borghuis BG, Sun XR, et al. Optimization of a GCaMP calcium indicator for neural activity imaging. J. Neurosci. 2012; 32:13819–13840. [PubMed: 23035093]

Albrecht DR, Bargmann CI. High-content behavioral analysis of *Caenorhabditis elegans* in precise spatiotemporal chemical environments. Nat. Methods. 2011

Atema J. Chemical signals in the marine environment: dispersal, detection, and temporal signal analysis. Proc. Natl. Acad. Sci. U. S. A. 1995; 92:62–66. [PubMed: 7816848]

Bähner M, Frechter S, Da Silva N, Minke B, Paulsen R, Huber A. Light-regulated subcellular translocation of *Drosophila* TRPL channels induces long-term adaptation and modifies the light-induced current. Neuron. 2002; 34:83–93. [PubMed: 11931743]

Bargmann CI. Comparative chemosensation from receptors to ecology. Nature. 2006; 444:295–301. [PubMed: 17108953]

Bargmann CI, Hartwieg E, Horvitz HR. Odorant-selective genes and neurons mediate olfaction in *C. elegans*. Cell. 1993; 74:515–527. [PubMed: 8348618]

Benhamou S, Bovet P. How animals use their environment: a new look at kinesis. Anim. Behav. 1989; 38:375–383.

Berg HC, Brown DA. Chemotaxis in *Escherichia coli* analysed by three-dimensional tracking. Nature. 1972; 239:500–504. [PubMed: 4563019]

Bielas SL, Silhavy JL, Brancati F, Kisseleva MV, Al-Gazali L, Sztriha L, Bayoumi RA, Zaki MS, Abdel-Aleem A, Rosti RO, et al. Mutations in INPP5E, encoding inositol polyphosphate-5-phosphatase E, link phosphatidyl inositol signaling to the ciliopathies. Nat. Genet. 2009; 41:1032–1036. [PubMed: 19668216]

Bloomfield SA, Völgyi B. The diverse functional roles and regulation of neuronal gap junctions in the retina. Nat. Rev. Neurosci. 2009; 10:495–506. [PubMed: 19491906]

Carandini M, Heeger DJ. Normalization as a canonical neural computation. Nat. Rev. Neurosci. 2011

Chalasani SH, Chronis N, Tsunozaki M, Gray JM, Ramot D, Goodman MB, Bargmann CI. Dissecting a circuit for olfactory behaviour in *Caenorhabditis elegans*. Nature. 2007; 450:63–70. [PubMed: 17972877]

Chalasani SH, Kato S, Albrecht DR, Nakagawa T, Abbott LF, Bargmann CI. Neuropeptide feedback modifies odor-evoked dynamics in *Caenorhabditis elegans* olfactory neurons. Nat. Neurosci. 2010; 13:615–621. [PubMed: 20364145]

Chou JH, Bargmann CI, Sengupta P. The *Caenorhabditis elegans odr-2* gene encodes a novel Ly-6-related protein required for olfaction. Genetics. 2001; 157:211–224. [PubMed: 11139503]

Dunn FA, Lankheet MJ, Rieke F. Light adaptation in cone vision involves switching between receptor and post-receptor sites. Nature. 2007; 449:603–606. [PubMed: 17851533]

Franz MO, Mallot HA. Biomimetic robot navigation. Robot. Auton. Syst. 2000; 30:133–153.

Fujiwara T, Kazawa T, Sakurai T, Fukushima R, Uchino K, Yamagata T, Namiki S, Haupt SS, Kanzaki R. Odorant concentration differentiator for intermittent olfactory signals. J. Neurosci. 2014; 34:16581–16593. [PubMed: 25505311]

Geffen MN, Broome BM, Laurent G, Meister M. Neural encoding of rapidly fluctuating odors. Neuron. 2009; 61:570–586. [PubMed: 19249277]

Goodman MB, Hall DH, Avery L, Lockery SR. Active currents regulate sensitivity and dynamic range in *C. elegans* neurons. Neuron. 1998; 20:763–772. [PubMed: 9581767]

Hilliard MA, Apicella AJ, Kerr R, Suzuki H, Bazzicalupo P, Schafer WR. In vivo imaging of *C. elegans* ASH neurons: cellular response and adaptation to chemical repellents. EMBO J. 2004; 24:63–72. [PubMed: 15577941]

Hires SA, Tian L, Looger LL. Reporting neural activity with genetically encoded calcium indicators. Brain Cell Bio. 2008; 36:69–86. [PubMed: 18941901]

Iino Y, Yoshida K. Parallel use of two behavioral mechanisms for chemotaxis in *Caenorhabditis elegans*. J. Neurosci. 2009; 29:5370. [PubMed: 19403805]

Inglis, PN.; Ou, G.; Leroux, MR.; Scholey, JM. The sensory cilia of *Caenorhabditis elegans* (March 8, 2007). In: WormBook. , editor. The *C. elegans* Research Community. 2007. http://www.wormbook.org

Izquierdo EJ, Lockery SR. Evolution and analysis of minimal neural circuits for klinotaxis in *Caenorhabditis elegans*. J. Neurosci. 2010; 30:12908–12917. [PubMed: 20881110]

Jacoby M, Cox JJ, Gayral S, Hampshire DJ, Ayub M, Blockmans M, Pernot E, Kisseleva MV, Compère P, Schiffmann SN, et al. INPP5E mutations cause primary cilium signaling defects, ciliary instability and ciliopathies in human and mouse. Nat. Genet. 2009; 41:1027–1031. [PubMed: 19668215]

Joesch M, Schnell B, Raghu SV, Reiff DF, Borst A. ON and OFF pathways in *Drosophila* motion vision. Nature. 2010; 468:300–304. [PubMed: 21068841]

Kato S, Xu Y, Cho CE, Abbott LF, Bargmann CI. Temporal responses of *C. elegans* chemosensory neurons are preserved in behavioral dynamics. Neuron. 2014; 81:616–628. [PubMed: 24440227]

Ke J-B, Wang YV, Borghuis BG, Cembrowski MS, Riecke H, Kath WL, Demb JB, Singer JH. Adaptation to background light enables contrast coding at rod bipolar cell synapses. Neuron. 2014; 81:388–401. [PubMed: 24373883]

Klapoetke NC, Murata Y, Kim SS, Pulver SR, Birdsey-Benson A, Cho YK, Morimoto TK, Chuong AS, Carpenter EJ, Tian Z, et al. Independent optical excitation of distinct neural populations. Nat. Methods. 2014; 11:338–346. [PubMed: 24509633]

Krzyzanowski MC, Brueggemann C, Ezak MJ, Wood JF, Michaels KL, Jackson CA, Juang BT, Collins KD, Yu MC, L'Etoile ND, Ferkey DM. The C. elegans cGMP-dependent protein kinase EGL-4 regulates nociceptive behavioral sensitivity. PLoS Genet. 2013; 9:e1003619. [PubMed: 23874221]

Kunitomo H, Sato H, Iwata R, Satoh Y, Ohno H, Yamada K, Iino Y. Concentration memory-dependent synaptic plasticity of a taste circuit regulates salt concentration chemotaxis in *Caenorhabditis elegans*. Nat. Commun. 2013; 4:2210. [PubMed: 23887678]

Lanjuin A, VanHoven MK, Bargmann CI, Thompson JK, Sengupta P. Otx/otd homeobox genes specify distinct sensory neuron identities in *C. elegans*. Developmental Cell. 2003; 5:621–633. [PubMed: 14536063]

Larsch J, Ventimiglia D, Bargmann CI, Albrecht DR. High-throughput imaging of neuronal activity in *Caenorhabditis elegans*. Proc. Natl. Acad. Sci. 2013; 110:E4266–E4273. [PubMed: 24145415]

Liu Q, Hollopeter G, Jorgensen EM. Graded synaptic transmission at the *Caenorhabditis elegans* neuromuscular junction. Proc. Natl. Acad. Sci. U.S.A. 2009; 106:10823–10828. [PubMed: 19528650]

Lukacs V, Thyagarajan B, Varnai P, Balla A, Balla T, Rohacs T. Dual regulation of TRPV1 by phosphoinositides. J. Neurosci. 2007; 27:7070–7080. [PubMed: 17596456]

Luo L, Wen Q, Ren J, Hendricks M, Gershow M, Qin Y, Greenwood J, Soucy ER, Klein M, Smith-Parker HK, et al. Dynamic encoding of perception, memory, and movement in a *C. elegans* chemotaxis circuit. Neuron. 2014; 82:1115–1128. [PubMed: 24908490]

Matsuura T, Izumi J, Nicki M, Nagaya H, Kobayashi Y. Sensory interaction between attractant diacetyl and repellent 2-nonanone in *Caenorhabditis elegans*. J. Exp. Zool A Ecol. Genet. Physiol. 2013; 319:285–295. [PubMed: 23580469]

Montell C. *Drosophila* visual transduction. Trends Neurosci. 2012; 35:356–363. [PubMed: 22498302]

Neher E. The use of fura-2 for estimating Ca buffers and Ca fluxes. Neuropharmacology. 1995; 34:1423–1442. [PubMed: 8606791]

Olsen SR, Bhandawat V, Wilson RI. Divisive normalization in olfactory population codes. Neuron. 2010; 66:287–299. [PubMed: 20435004]

Di Paolo G, De Camilli P. Phosphoinositides in cell regulation and membrane dynamics. Nature. 2006; 443:651–657. [PubMed: 17035995]

Petersen CI, McFarland TR, Stepanovic SZ, Yang P, Reiner DJ, Hayashi K, George AL, Roden DM, Thomas JH, Balser JR. In vivo identification of genes that modify ether-a-go-go-related gene activity in *Caenorhabditis elegans* may also affect human cardiac arrhythmia. Proc. Natl. Acad. Sci. U. S. A. 2004; 101:11773–11778. [PubMed: 15280551]

Pierce-Shimomura JT, Morse TM, Lockery SR. The fundamental role of pirouettes in *Caenorhabditis elegans* chemotaxis. J. Neurosci. 1999; 19:9557. [PubMed: 10531458]

Qin H, Burnette DT, Bae Y-K, Forscher P, Barr MM, Rosenbaum JL. Intraflagellar Transport Is Required for the Vectorial Movement of TRPV Channels in the Ciliary Membrane. Curr. Biol. 2005; 15:1695–1699. [PubMed: 16169494]

Reisert J, Zhao H. Perspectives on: Information and coding in mammalian sensory physiology: Response kinetics of olfactory receptor neurons and the implications in olfactory coding. J. Gen. Physiol. 2011; 138:303–310. [PubMed: 21875979]

Richmond JE, Davis WS, Jorgensen EM. UNC-13 is required for synaptic vesicle fusion in *C. elegans*. Nat. Neurosci. 1999; 2:959–964. [PubMed: 10526333]

Rieke F, Rudd ME. The challenges natural images pose for visual adaptation. Neuron. 2009; 64:605–616. [PubMed: 20005818]

Riffell JA, Abrell L, Hildebrand JG. Physical processes and real-time chemical measurement of the insect olfactory environment. J. Chem. Ecol. 2008; 34:837–853. [PubMed: 18548311]

Roayaie, K. PhD Thesis. San Francisco: The University of California; 1996. Studies of chemosensory signal transduction in *Caenorhabditis elegans*.

Satoh Y, Sato H, Kunitomo H, Fei X, Hashimoto K, Iino Y. Regulation of experience-dependent bidirectional chemotaxis by a neural circuit switch in *Caenorhabditis elegans*. J. Neurosci. 2014; 34:15631–15637. [PubMed: 25411491]

Sengupta P, Colbert HA, Bargmann CI. The *C. elegans* gene *odr-7* encodes an olfactory-specific member of the nuclear receptor superfamily. Cell. 1994; 79:971–980. [PubMed: 8001144]

Sengupta P, Chou JH, Bargmann CI. *odr-10* Encodes a Seven Transmembrane Domain Olfactory Receptor Required for Responses to the Odorant Diacetyl. Cell. 1996; 84:875–887. [PubMed: 8601311]

Shinkai Y, Yamamoto Y, Fujiwara M, Tabata T, Murayama T, Hirotsu T, Ikeda DD, Tsunozaki M, Iino Y, Bargmann CI, et al. Behavioral choice between conflicting alternatives is regulated by a receptor guanylyl cyclase, GCY-28, and a receptor tyrosine kinase, SCD-2, in AIA interneurons of *Caenorhabditis elegans*. J. Neurosci. 2011; 31:3007–3015. [PubMed: 21414922]

Shoval O, Goentoro L, Hart Y, Mayo A, Sontag E, Alon U. Fold-change detection and scalar symmetry of sensory input fields. Proc. Natl. Acad. Sci. USA. 2010; 107:15995–16000. [PubMed: 20729472]

Sourjik V. Receptor clustering and signal processing in *E. coli* chemotaxis. Trends Microbiol. 2004; 12:569–576. [PubMed: 15539117]

Suzuki H, Thiele TR, Faumont S, Ezcurra M, Lockery SR, Schafer WR. Functional asymmetry in *Caenorhabditis elegans* taste neurons and its computational role in chemotaxis. Nature. 2008; 454:114–117. [PubMed: 18596810]

Tian L, Hires SA, Mao T, Huber D, Chiappe ME, Chalasani SH, Petreanu L, Akerboom J, McKinney SA, Schreiter ER, et al. Imaging neural activity in worms, flies and mice with improved GCaMP calcium indicators. Nat. Methods. 2009; 6:875–881. [PubMed: 19898485]

Vergassola M, Villermaux E, Shraiman BI. "Infotaxis" as a strategy for searching without gradients. Nature. 2007; 445:406–409. [PubMed: 17251974]

Wakabayashi T, Kimura Y, Ohba Y, Adachi R, Satoh Y, Shingai R. In vivo calcium imaging of OFF-responding ASK chemosensory neurons in *C. elegans*. Biochim. Biophys. Acta. 2009; 1790:765–769. [PubMed: 19362117]

Wark B, Lundstrom BN, Fairhall A. Sensory adaptation. Curr. Opin. Neurobiol. 2007; 17:423–429. [PubMed: 17714934]

Wässle H. Parallel processing in the mammalian retina. Nat. Rev. Neurosci. 2004; 5:747–757. [PubMed: 15378035]

Weimer RM, Richmond JE, Davis WS, Hadwiger G, Nonet ML, Jorgensen EM. Defects in synaptic vesicle docking in *unc-18* mutants. Nat. Neurosci. 2003; 6:1023–1030. [PubMed: 12973353]

White JG, Southgate E, Thomson JN, Brenner S. The structure of the nervous system of the nematode *Caenorhabditis elegans*. Philos. Trans. R. Soc. Lond. B. Biol. Sci. 1986; 314:1–340. [PubMed: 22462104]

Wicks SR, de Vries CJ, van Luenen HGAM, Plasterk RHA. CHE-3, a cytosolic dynein heavy chain, is required for sensory cilia structure and function in *Caenorhabditis elegans*. Dev. Biol. 2000; 221:295–307. [PubMed: 10790327]

Wilson RI. Early olfactory processing in *Drosophila*: mechanisms and principles. Annu. Rev. Neurosci. 2013; 36:217–241. [PubMed: 23841839]

Zhu P, Frank T, Friedrich RW. Equalization of odor representations by a network of electrically coupled inhibitory interneurons. Nat. Neurosci. 2013; 16:1678–1686. [PubMed: 24077563]
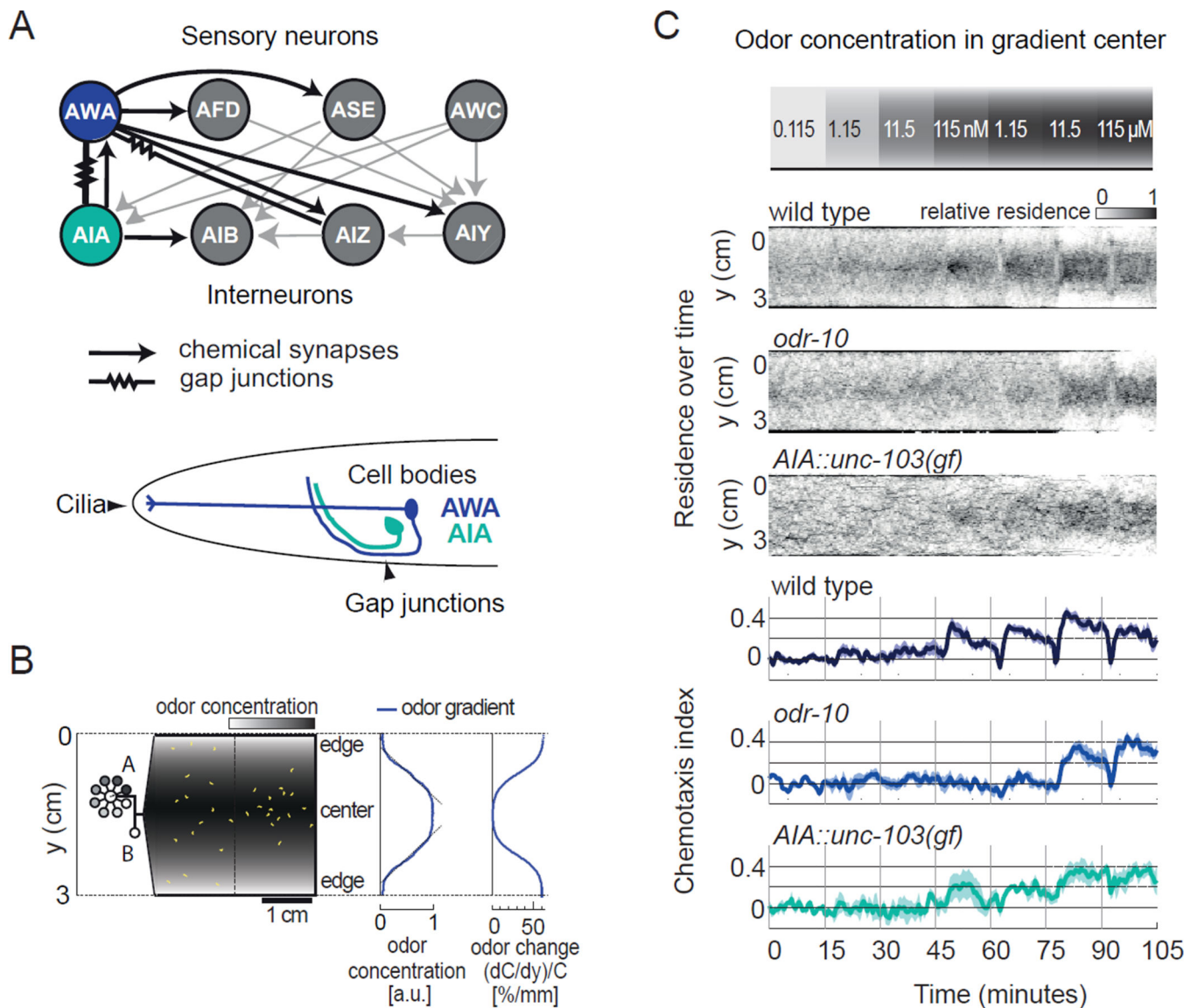
Figure 1. A neural circuit for chemotaxis towards defined concentrations of diacetyl

a) The AWA circuit. Top, part of the *C. elegans* wiring diagram (White et al., 1986), emphasizing synaptic connections between AWA olfactory neurons and other sensory neurons and interneurons. Each sensory neuron has additional targets, and each interneuron integrates input from additional sensory neurons. Bottom, schematic illustration of AWA and AIA. AWA detects odors via cilia on the distal sensory dendrite and forms axonal gap junctions with AIA interneurons.

b) Schematic of microfluidic behavioral device in which sigmoidal odor gradients of known diacetyl concentrations are delivered to freely moving animals. Diacetyl concentrations at the outer edges are held constant at 0.115 nM via inlet B. Peak odor concentration is selected using a computer controlled distribution valve via inlet A. Middle, odor concentration profile. Gradient in arbitrary units (a.u.) scales with peak odor concentration, and the slope of much of the gradient is near-linear. Right, concentration change per mm

experienced by an animal moving toward the center of the arena; animals move at about 0.2 mm/second. See also Supplemental Movie 1.

c) Behavior of wild-type and mutant animals in diacetyl gradients. The peak diacetyl concentration was increased ten-fold as indicated every 15 minutes (top). Middle three panels, distribution of animals in the device expressed as a density function of residence over time. Bottom three panels, a mean chemotaxis index represented the location of animals in the device during 2 s time bins (continuous scale from –1 at device edge to +1 at device center). *odr-10(ky32)* mutants lack the AWA diacetyl receptor. *unc-103(gf)* strains express a hyperactive K+ channel in the AIA neurons under the *gcy-28d* promoter. Shading represents s.e.m. n = 4–6 assays with 20–30 animals per genotype.
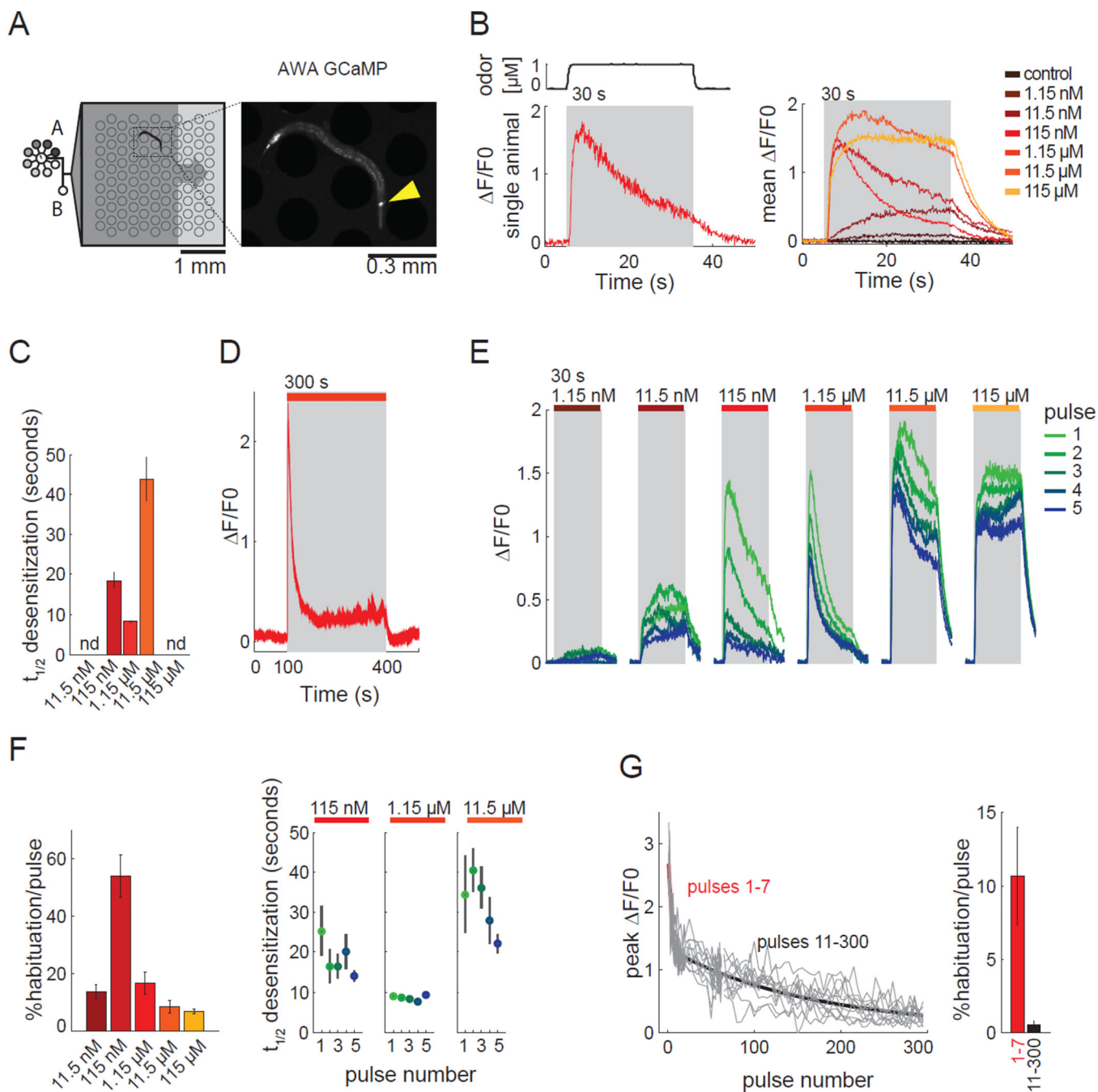
Figure 2. AWA calcium dynamics are shaped by odor concentration and history

a) Schematic of 3×3 mm microfluidic imaging device, illustrating flow of odor past animals in a pulse assay, and camera frame showing GCaMP2.2b fluorescence in AWA sensory neuron (arrowhead).

b) AWA calcium response to 30 s pulses of diacetyl. Top left, odor switches from 10% to 90% final concentration within 1 s, based on dye measurement. Bottom left, single trace at 1.15 μM. Right, average of multiple trials, n=9 animals, 5 pulses at each concentration.

c) AWA desensitization rates within 30 s odor pulses (data from b). nd, not detectable.

d) AWA calcium response to 5 min pulse of 1.15 μM diacetyl; trace shading = s.e.m. n=12 animals, 1 trial each.

e) AWA calcium responses to five successive 30 s pulses of odor at each concentration. Green, first pulse; blue, last pulse. n=9 animals tested across all concentrations.

f) (Left) Habituation of peak AWA fluorescence between pulses. (Right) Desensitization rates within pulses, with repeated pulses at the same concentration. Error bars, s.e.m. n=9 animals.

g) Peak AWA fluorescence to 5 s pulses of 1.15 μM diacetyl delivered once every 60 s. Gray: 11 individual animals, red and black: best fit to the equation $y(t) = y_0 * \exp(-k*t)$ separately during two phases: 1, pulses 1–7, 2, pulses 11–300. Habituation rate k represents decrease of peak AWA fluorescence per 5 s pulse. Error bars, s.e.m. n=11 animals.
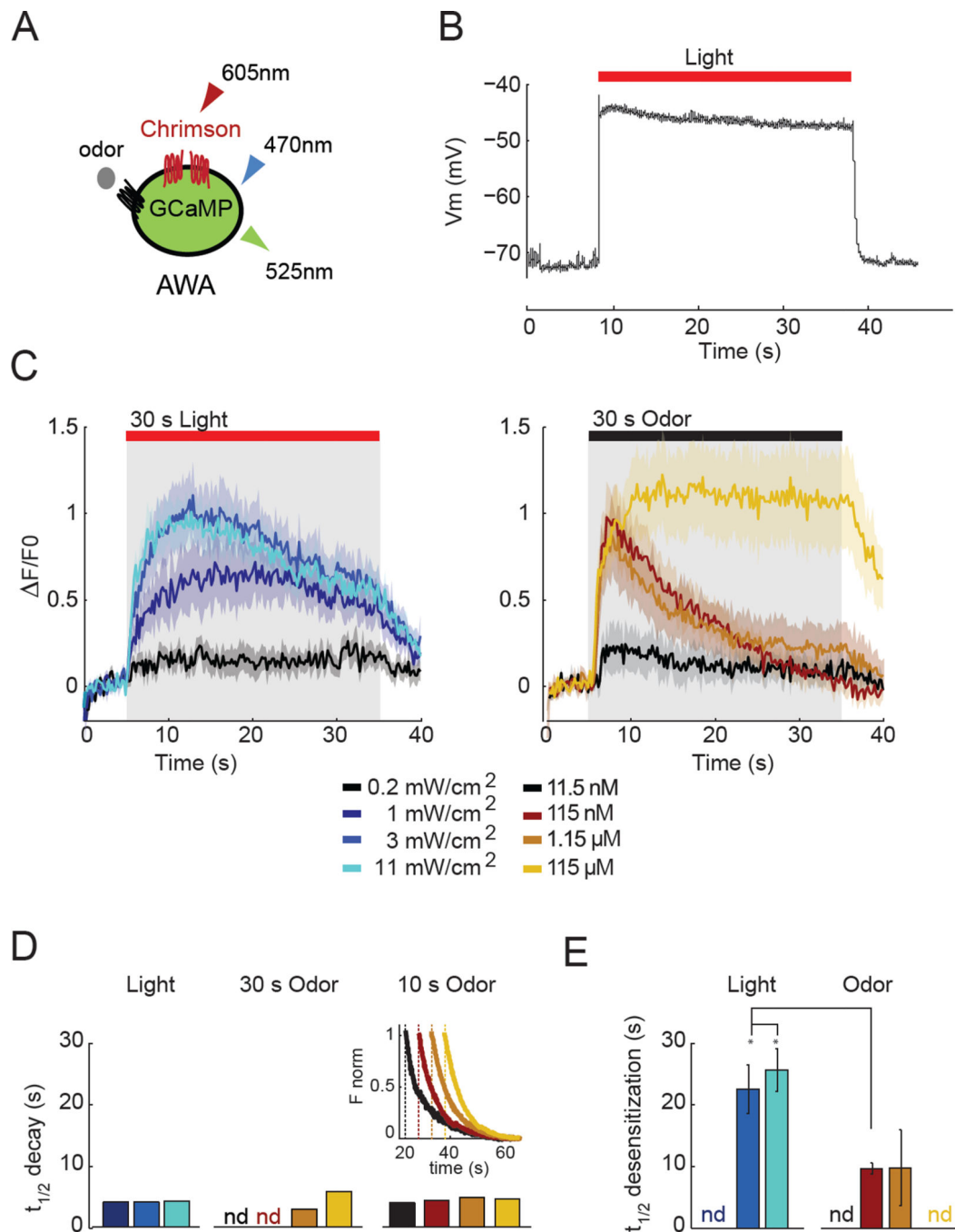
Figure 3. Contribution of voltage to GCaMP dynamics

a) Coexpression of the red-shifted Chrimson cation channel with GCaMP2.2b in AWA. Red light excites Chrimson to depolarize AWA; blue light excites GCaMP2.2b in AWA.

b) Electrophysiological responses of AWA neuron to depolarization by Chrimson. Representative trace in current clamp during 30 s of illumination; n=7 traces.

c) (Left) AWA calcium response during Chrimson stimulation for 30 seconds at different light intensities. (Right) AWA calcium response during odor stimulation of the same

animals. Shading represents s.e.m. Note that desensitization results in a faster time to peak, a typical feature of sensory systems. n=10 animals.

d) Decay of AWA GCaMP fluorescence after Chrimson illumination and after removal of a 30s or 10s odor stimulus. Colors indicate stimuli as in **(c)**. Inset: normalized fluorescence after 10 s odor stimuli, time shifted to illustrate similar rates of decay. Data from 10 s odor are in Figure 4a.

e) Rates of desensitization in continuous light (Chrimson) or continuous odor from (**c**). For other odor stimuli, see Figure 2. For additional GCaMP indicators and further discussion of calcium signaling dynamics, see Figure S1.
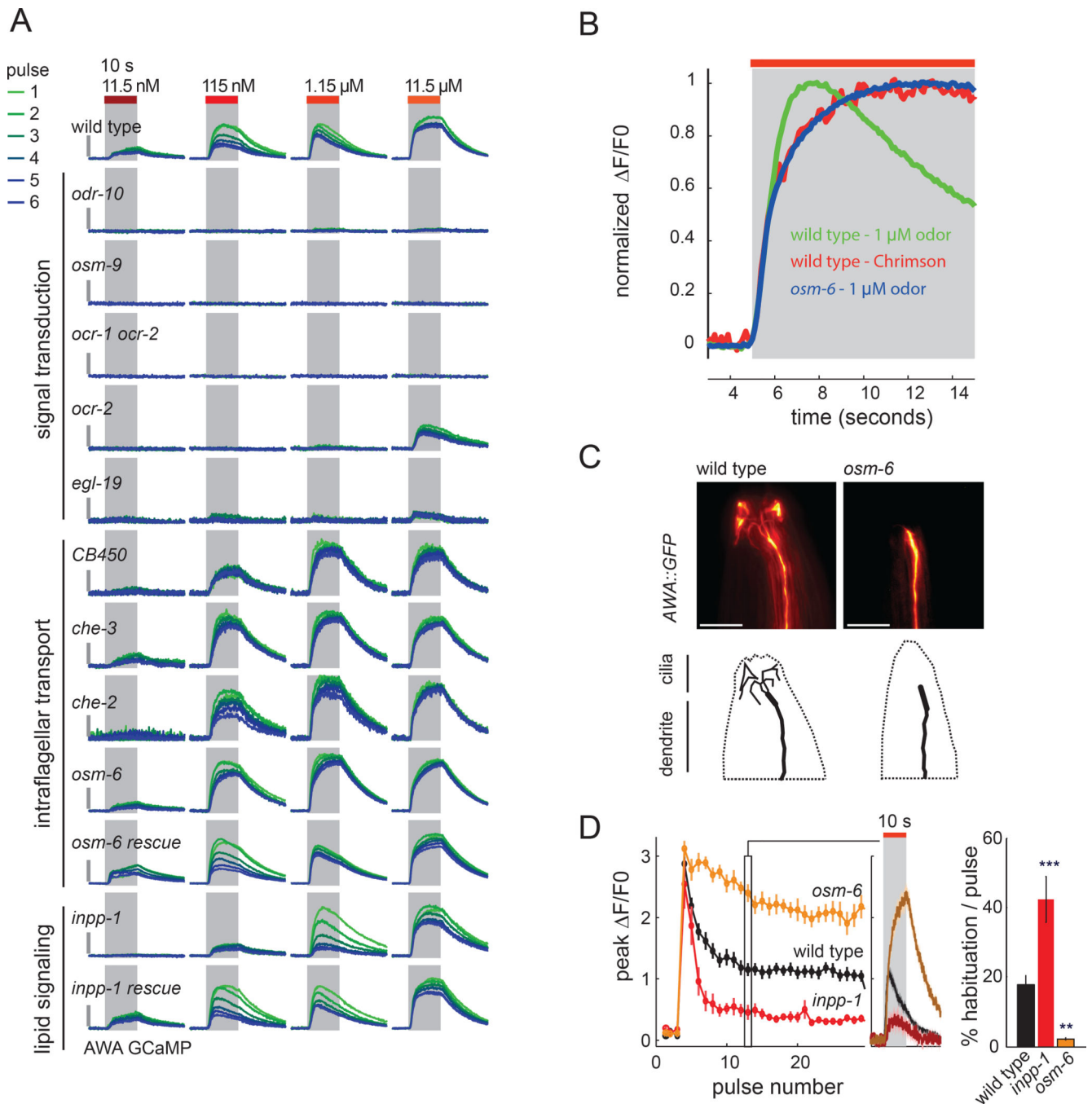
Figure 4. Intraflagellar transport and inositol lipids modulate AWA responses

a) AWA calcium response during odor stimulation in olfactory signal transduction mutants, IFT mutants, and *inpp-1(ky121)* mutants. Gray vertical bars indicate 1 ΔF/F0. Note that these are 10 s pulses, not 30 s as in Figure 2. See also Figure S2, S3.

b) AWA calcium dynamics in wild-type and IFT mutants. AWA calcium responses to 1.15 µM diacetyl or Chrimson (11 mW/cm^2), normalized to peak calcium. Rapid desensitization to odor is not observed in Chrimson and *osm-6;* accelerated time-to-peak is driven by rapid desensitization (Figure 3).

c) Fluorescence z-stack projection of anterior tip of representative animals expressing GFP in AWA sensory neurons showing sensory dendrite and cilia. Scale bar, 10 μm.

d) Peak AWA calcium response and habituation rate for 10 s pulses of 1.15 μM diacetyl delivered once every 60 s. Traces in the center show AWA response during the tenth odor pulse. Error bars and shading represent s.e.m. n = 5–12 animals per genotype. **P<0.01, ***P<0.001 versus wild-type.
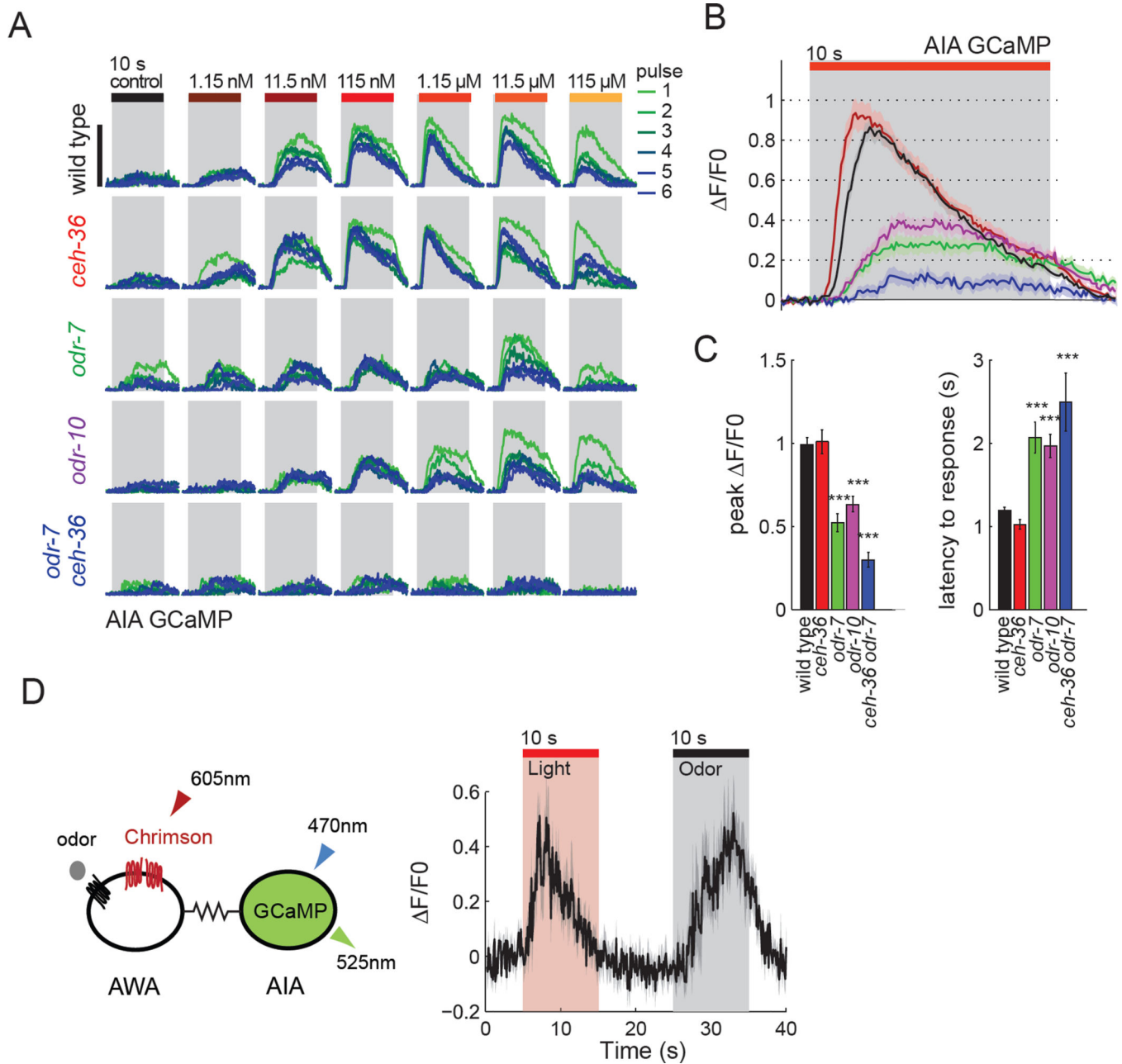
Figure 5. AIA integrates diacetyl inputs from AWA and other sensory neurons

a) AIA neurite calcium response to 10 s pulses of diacetyl, 6 pulses at each concentration, n=9–24 animals per genotype. Black bar indicates 1 ΔF/F0. AIA neurons express GCaMP5(D380Y). *ceh-36(ky640)* disrupts AWC and ASEL cell fate (Lanjuin et al., 2003). *odr-7(ky4)* disrupts AWA cell fate (Sengupta et al., 1994).

b) AIA neurite calcium response in different genotypes during 10 s pulses of 1.15 μM diacetyl, shading represents s.e.m. n = 9–24 animals per genotype. Color legend of genotypes matches panels a and c.

c) Peak AIA neurite calcium response (left) and latency to response (right) during 10 s pulses of 1.15 μM diacetyl. Latency is defined as time from start of odor pulse until

fluorescence levels exceed 2 standard deviations of baseline fluorescence. Error bars represent s.e.m. **P<0.01, ***P<0.001 versus wild type.

d) AWA to AIA signaling. Left, expression of the red-shifted Chrimson cation channel in AWA, and GCaMP5(D380Y) in AIA. Red light excites Chrimson to depolarize AWA; blue light excites GCaMP5. Right, AIA neurite calcium response to 10 s Chrimson stimulation of AWA (10 mW/cm^2) alternated with 10 s pulse of 11.5 nM diacetyl. Note that this odor concentration induces a slowly rising AIA response compared to higher concentrations (panel a). Shading represents s.e.m. n = 15 animals.
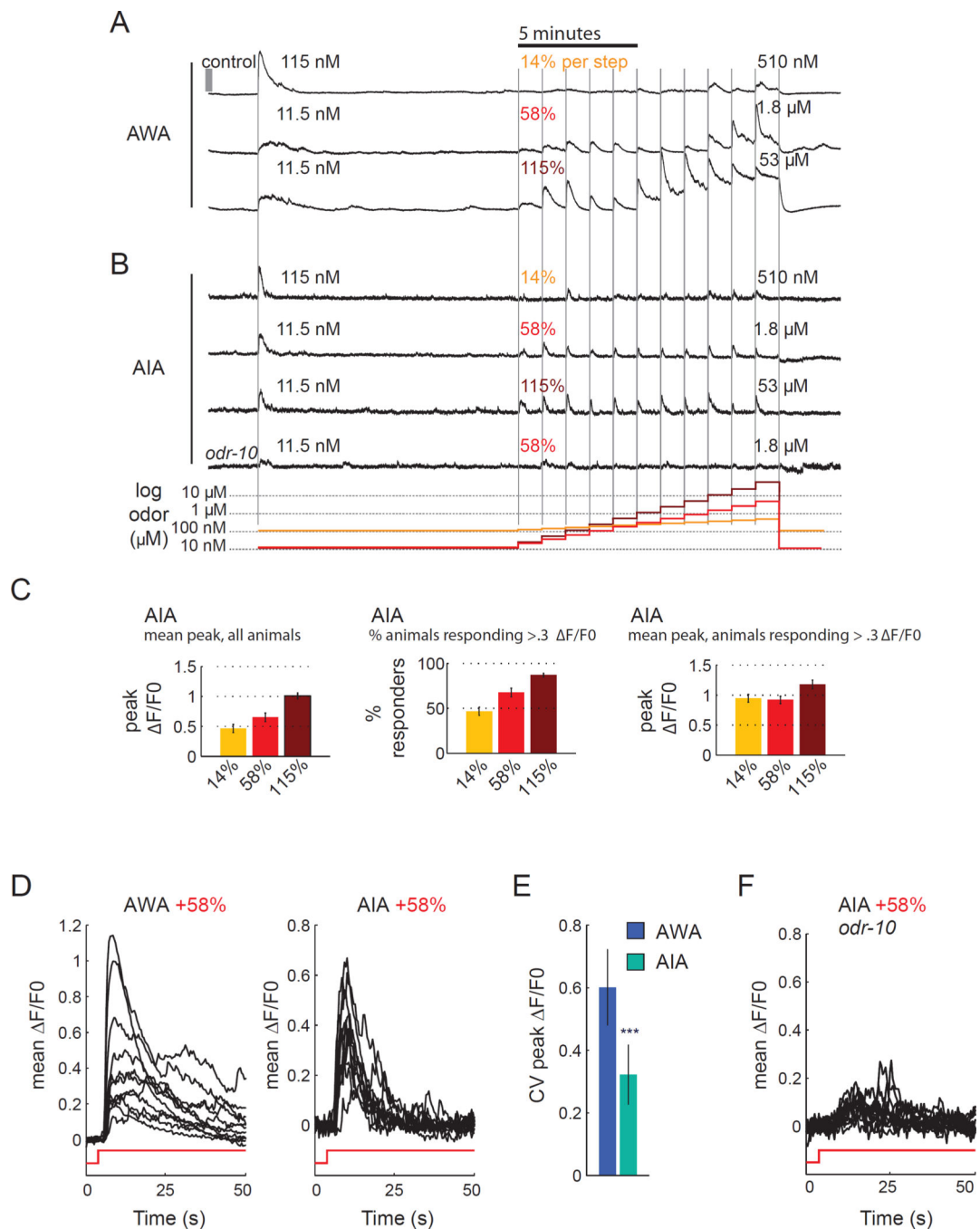
Figure 6. AIA normalizes AWA responses to small diacetyl increases

a,b) AWA calcium response **(a)** or AIA neurite calcium response **(b)** during eleven successive fold-change increases in odor concentration. Gray vertical bar indicates 1 ΔF/F0. Odor increase was 14%, 58% and 115% per step, starting from 115 nM, 11.5 nM, and 11.5 nM, respectively. Legend at bottom illustrates odor concentration at each step.

c) Larger odor steps from (b) increase the mean AIA response (left panel) and the probability of a response to each upstep (middle panel), but do not greatly increase the peak response magnitude (right panel).

d) Mean AWA and AIA calcium responses to each 58% fold-change increase, superimposed at the same gain. Note higher variability in AWA calcium response across concentrations. n=14–16 animals per step.

e) Coefficient of variation of AWA and AIA calcium responses during 58% fold-change increase. Error bars represent s.e.m. n = 14–16 animals; ***P<0.001 vs. AWA.

f) AIA neurons in *odr-10* mutants do not respond to 58% fold-change diacetyl increases (n=10 animals).
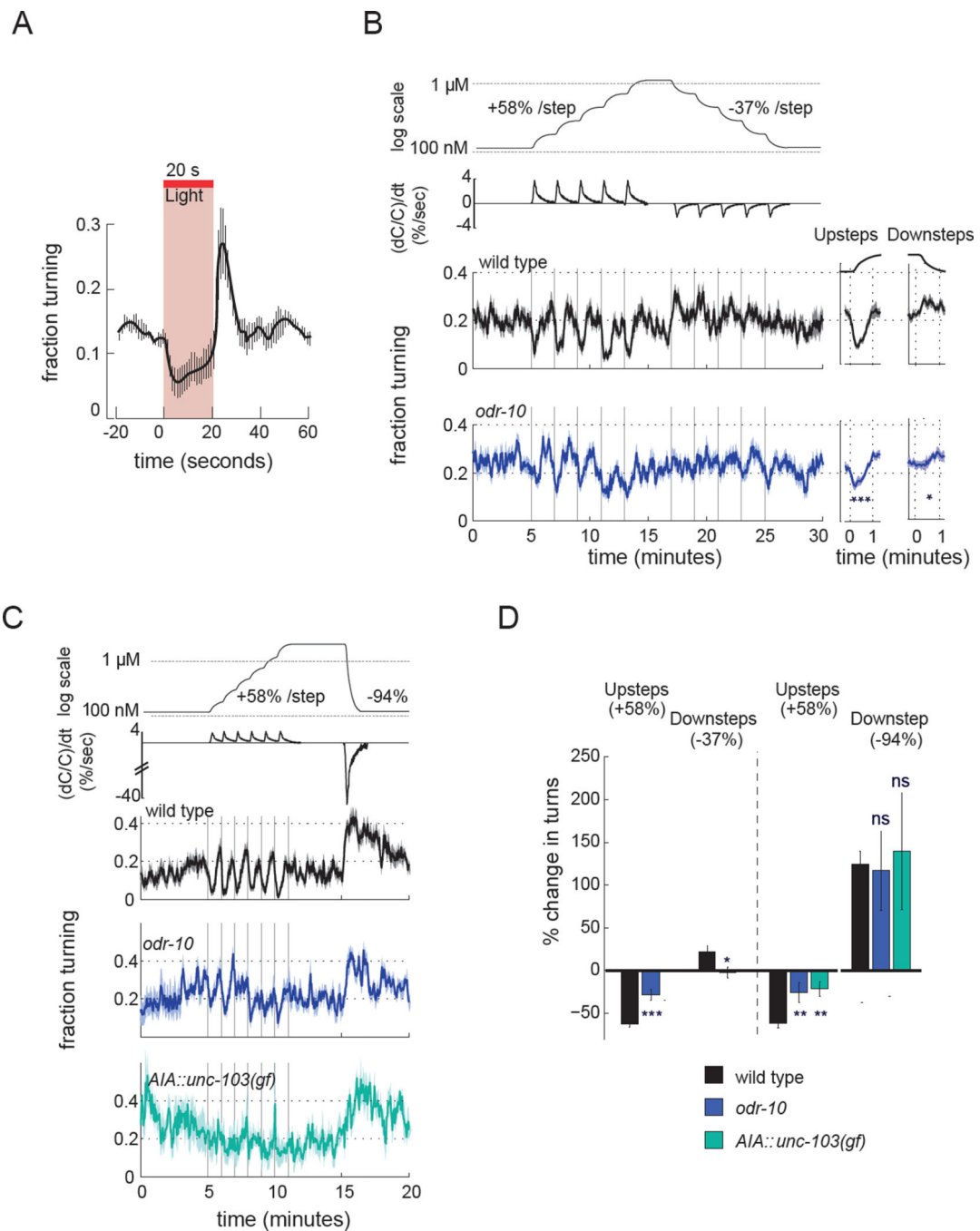
Figure 7. AWA and AIA drive behavioral responses to small diacetyl increases

a) Behavior of animals expressing Chrimson in AWA during and after 20 s of light stimulation. Animals were filmed as they moved freely on agar plates, and instantaneous turning frequencies (encompassing reversals and omega turns) were scored automatically in 1 s time bins. Error bars represent s.e.m. n = 3 experiments, 15–20 animals each.

b) Behavioral responses of freely-moving animals to fold-change odor increases and decreases, delivered once per minute in microfluidic arenas. Odor concentrations (shown on log scale) and the change in relative odor concentration over time, (dC/C)/dt are shown at

top; fold-changes result in a constant (dC/C)/dt. Instantaneous fraction of wild-type and *odr-10* animals turning during the diacetyl stimulation protocol is shown at bottom. At right, average response over all fold-change steps. A 58% increase corresponds to a 37% decrease per step. Shading represents s.e.m. n=8 assays with 20–30 animals per genotype, 2 repeats per assay. ***, different from wild-type at P<0.001; *, different from wild-type at P<0.05.

c) Behavioral responses of freely-moving animals to 58% fold-change odor increases and a large 94% step decrease. Odor concentrations and dC/dt are shown at top. Data show instantaneous fraction of animals turning during the diacetyl stimulation protocol. n=4–10 assays with 20–30 animals per genotype.

d) Suppression of turning during 58% upsteps and enhancement during large but not small downsteps in experiments in (b) and (c). Bars represent the average change in peak response over all fold-change increases or decreases. Error bars represent s.e.m. *P<0.05; **P<0.01;***P<0.001 compared to wild type; ns not significant.